



Degradation of Fuel Cell Membrane Electrode Assemblies from Buses Operated More than 25,000 h

Harsh Srivastav,^{1,2} Arthur Dizon,² Lynda Amichi,³ Mike L. Perry,⁴ Ali Aboobaker Sadhakkathullahil,² Grace Lau,² Catherine M. Weiss,² Brice Florey,³ Douglas I. Kushner,² Matthew Wilson,⁴ Dave A. Cullen,³ Mike Gorman,⁴ Clayton J. Radke,¹ Adam Z. Weber,² and Rangachary Mukundan^{2,*,z}

This study investigates the performance losses and degradation of proton-exchange-membrane fuel-cell stacks taken from the Alameda Contra Costa Transit District (AC Transit) bus system (Alameda and Contra Costa counties, California, United States) that were operated for over 25,000 h. Here, we focus on the origin of differences in electrochemical performance between beginning-of-life (BOL) and end-of-life states as well as diagnostic data acquired during the lifetime of the buses. In doing so, we employ *in-* and *ex-* situ characterization methods such as polarization curves, electrochemical impedance spectroscopy, electron microscopy, and X-ray characterization. Uniform degradation of the catalyst layer including Pt agglomeration/migration and electrode thinning was observed in all of the post-teardown measurements compared to BOL materials resulting from years of field operation. Despite these changes, the measured post-teardown performance suggests a sufficient output for the expected load, which indicate factors other than degradation of the membrane-electrode assemblies (MEAs) are likely responsible for the decommissioning of the stacks. The findings indicate that these MEA materials can enable long lifetime in fuel-cell vehicles, if the MEAs are not subjected to adverse operating conditions. The results also highlight the need for more in-vehicle diagnostics to maximize the lifetime of fuel cell vehicle (FCV) powerplants.

© 2025 The Author(s). Published on behalf of The Electrochemical Society by IOP Publishing Limited. This is an open access article distributed under the terms of the Creative Commons Attribution 4.0 License (CC BY, https://creativecommons.org/licenses/by/4.0/), which permits unrestricted reuse of the work in any medium, provided the original work is properly cited. [DOI: 10.1149/1945-7111/ade82b]

Manuscript submitted December 30, 2024; revised manuscript received June 12, 2025. Published July 9, 2025. This paper is part of the JES Focus Issue on Proton Exchange Membrane Fuel Cell and Proton Exchange Membrane Water Electrolyzer Durability III.

Supplementary material for this article is available online

Hydrogen fuel cells have the potential for increased efficiency over traditional energy conversion devices and can result in greatly decreased emissions of harmful criteria pollutants (such as carbon monoxide, nitrogen oxides, particulate matter) compared to combustion engines. 1,2 During normal operation, the byproduct of a polymer electrolyte membrane fuel cell (PEMFC) is simply water, which can be harmlessly released into the environment, avoiding any $\rm CO_2$ emissions. Fuel cells directly convert the chemical energy of the hydrogen fuel into electrical energy that can be utilized as a power source directly for many applications. For all of these reasons, fuel cells present a promising emerging technology for both stationary power generation and transportation applications, especially for heavy-duty vehicles. 3,4

Despite these advantages, fuel cell vehicles face challenges that must be addressed for widespread adoption. First, the production, storage, and distribution of hydrogen remains costly and energy-intensive, relying primarily on natural gas sources. Advancing technology to drive the production and improve the efficiency of low carbon intensive hydrogen—hydrogen produced via electrolysis powered by renewable energy sources—becomes critical for alleviating the reliance on non-renewable energy supplies. Additionally, the development of hydrogen refueling infrastructure and advancements in fuel cell technology are essential for scaling up adoption and reducing costs. The hydrogen industry is at a pivotal moment with governments worldwide promoting hydrogen energy through subsidies and initiatives, and several major automakers, such as Toyota, Hyundai, and Honda, offering commercial Fuel Cell Vehicle (FCV). 10-12 Hydrogen-fueled FCVs offer a pathway toward

^zE-mail: rmukundan@lbl.gov

a zero-emission future, but their success will depend on overcoming key technical and economic barriers including the lack of data and understanding of the durability of the cells and components over time in real-world operation.

The Alameda Contra Costa Transit District (AC Transit) operates a fleet of 626 buses to transport residents in the Alameda and Contra Costa counties of California. Of the 626 buses commissioned, AC Transit operated 13 fuel-cell buses, which were fully electric hybrids using fuel cell and battery, under its Legacy Fuel Cell Bus Study, denoted as FC4 to FC16. ^{13,14} This included an initial deployment of three Van Hool A330 fuel cell buses in 2006 and a later expansion of 10 additional Van Hool fuel cell buses in 2010–2011. ¹⁵ The Legacy fleet had an average operating lifetime of 25,763 h with three of the buses reaching over 30,000 h without requiring significant maintenance. The performance of these buses was measured periodically throughout their lifetime when brought in for maintenance. FC7 and FC12 (one of the buses studied in this work) had lower mileages because spare fuel-cell components were installed after the original stacks were decommissioned. FC4 was part of the additional expansion fleet in 2010. ¹⁴

This data and the stacks from two different fuel cell buses were donated by AC Transit to the authors of this work for the purpose of providing insight into the degradation of the fuel-cell stacks operated in the field. Each bus contained two stacks of 290 PEMFC Membrane Electrode Assemblies (MEAs). Each MEA has an active area of $420~\text{cm}^2$ and is comprised of an $18~\mu\text{m}$ membrane 16 with symmetric anode and cathode catalyst layers with a nominal loading of $0.4~\text{mg}_{\text{Pt}}~\text{cm}^{-2}$ and $12~\mu\text{m}$ thickness manufactured by W. L. Gore & Associates, Inc. (Newark, DE, USA). At beginning-of-life (BOL), the Pt particle diameters were approximately 2~nm, and the stacks were operated at atmospheric exhaust pressure. The stacks employed microporous bipolar plates, or water transport plates (WTPs) and

¹Department of Chemical and Biomolecular Engineering, University of California, Berkeley, California, 94720, United States of America

²Energy Technologies Area, Lawrence Berkeley National Laboratory, Berkeley, California, 94720, United States of America ³Center for Nanophase Materials Science, Oak Ridge National Laboratory, Oak Ridge, Tennessee, 37830, United States of America

⁴Nimbus Power Systems, Inc., Groton, Connecticut, 06340, United States of America

^{*}Electrochemical Society Fellow.

were operated with hydrogen and air, as has been described elsewhere. ^{17,18} Figure 1 contains a photograph of a single stack, as well as a depiction of the geometry of the reactant streams. The anode flow field channels were straight and partitioned equally between the first and second passes. The cathode flow field channels contained an oblique flow section and were asymmetrically partitioned such that the first pass included slightly more than half the active area due to decrease in air flowrate from inlet to outlet. Further details of the stack design are contained in Fig. S1 in the SI.

Methods and Materials

Provided bus performance data analysis.—To facilitate comparison with fuel cell data obtained in the laboratory using BOL and end-of-life (EOL) MEAs, the data provided by AC Transit was filtered to only those files that contained stack voltage variation instead of voltage holds. These polarization curves largely contained only ohmic regime data (mostly between 0.5 V to 0.8 V), but this still presents invaluable field insights of working PEMFCs. The PEMFC performance was taken periodically over the course of the buses' lifetimes (over 10 years in the case of some of the buses). Although 13 different PEMFC buses were part of the Zero Emission program, the stacks from only two of these buses were provided for complete tear-down analysis. The two buses for which parts were physically provided for further testing were the stacks from buses FC4 and FC12. Both buses reached end of life due to their inability to deliver the minimum voltage required by the bus's powerconversion system. FC4 failed at 29,822 h over a period 11 years, 4 months and traveled for a total of 264,079 miles, while FC12 failed at 25,964 h over 7 years, 4 months (total miles traveled not included in end of life reported, but at least 185,000 miles). Figure S2 in the SI shows an example of an end of life (EOL) report provided by AC Transit.

The data analysis initially used a macro to aggregate the data for each bus (initially in.csv files) into sheets in a single Excel workbook, filtering out files that did not exhibit voltage differences greater than $20\,\mathrm{V}$ (or $0.034\,\mathrm{V}$ per fuel cell). The data was further

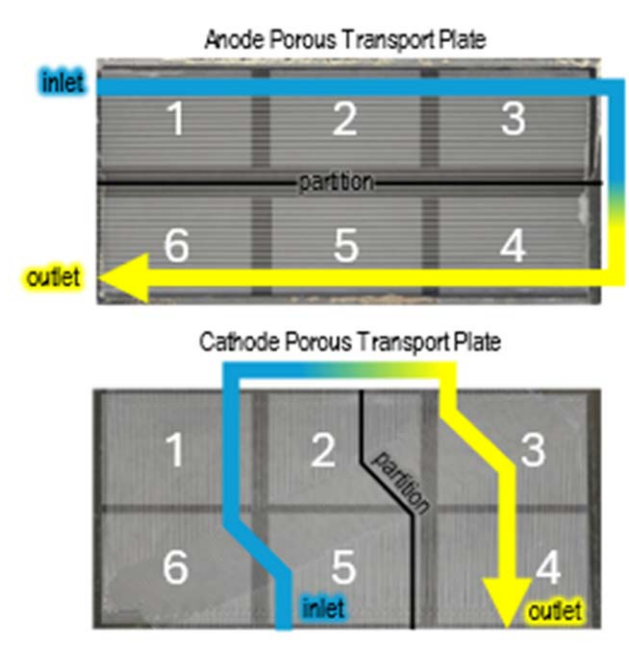
filtered by the anode backpressure to provide useful comparison, as the backpressure significantly impacts performance. ¹⁹ The workbooks were then processed using the Pandas library and saved as Pandas dataframes locally. As the data was perceived to be very noisy, a convolution filter was implemented to smooth the data over every 10 points. For all data that follows, the voltages were normalized by the number of cells (580 total for both stacks), while the current densities were normalized by the cross-sectional area (420 cm²).

Cell analysis.—We utilized a variety of experimental techniques to determine the root cause of the performance loss observed in the stacks. First, we obtained performance data through polarization curves, electrochemical impedance spectroscopy (EIS), cyclic voltammetry (CV), and mass activity measurements on MEAs harvested from the EOL stacks. Even though we were limited in the data taken throughout the lifetime of the bus to the ohmic regime, the polarization curves obtained from BOL and EOL MEAs included the kinetic, ohmic, and transport limited regimes. 20–22 Moreover, EIS allowed for additional analysis to identify contributions to performance loss from changes in membrane resistance, electrode kinetics, and mass transport. 23–29 The CVs were measured to determine the hydrogen underpotential deposition, which was used to calculate the electrochemical surface area (ECSA).

Additionally, we supplemented the above methods with imaging using electron microscopy. These techniques yield thicknesses of the layers involved, to monitor overall cell degradation. In addition, Pt particle size distributions are useful in accounting for Electrochemical Surface Area (ECSA) losses, since larger Pt particles result in a smaller available surface area. A summary of the experimental techniques and which cells they were performed on can be found in Table I.

Single-cell testing procedure.—Individual cells were tested on 850 and 840 fuel-cell test stations equipped with 885 potentiostats and automatic backpressure units (Scribner LLC, Southern Pines,





b

Figure 1. (a) A photograph of a stack with 290 cells is shown with the external fuel and air manifolds removed. The pipe shown jutting out of the stack in the front are water lines for the coolant. The anode side is facing the front (where the hydrogen enters the stack). (b) Depictions of the geometry of the reactant streams, which consisted of two passes across the MEA. External manifolds connect to channels in the bipolar plates. The anode plates used straight channels in the direction of the long side of the cell. (top) The cathode plate directed air in two passes with an asymmetric non-linear path (bottom). The MEA sampling regions were identified as regions 1 through 6. There were no partitions in the MEA.

Table I. Tabulation of MEA samples and the analyses performed. Sampling locations indicated in the identifier are from the cell areas shown in Fig. 1b, 50 cm^2 . MEA samples with the identifier (x/y) indicate that the sampling location was obtained from an area spanning areas x and y. A location of "NR" stands for not recorded.

Sample identifier	Cell	Location	Area (cm ²)	GDL material	Electrochemical analyses	Technique
BOL			5	Sigracet® 22BB	PC, ECSA	SEM
BOL			50	BOL Nimbus GDL	PC, ECSA	
270	270	NR	5	Sigracet® 22BB	PC, ECSA	
271-1	271	1	5	Sigracet® 22BB	PC, ECSA	SEM
271-4	271	4	5	Sigracet® 22BB	PC, ECSA	SEM
7	7		50	EOL GDL	PC, ECSA, EIS	SEM
7-1	7	1				TEM, PSD
7–6	7	6				TEM, PSD
165-1/6	165	1/6	50	EOL GDL	PC, ECSA, EIS	SEM
165-3/4	165	3/4	50	EOL GDL	PC, ECSA, EIS	SEM
74	74	NR	50	EOL GDL	PC, ECSA, EIS	
281	281	NR	50	EOL GDL	PC, ECSA, EIS	SEM
150	150	NR	50	EOL GDL	PC, ECSA, EIS	SEM
150	150	NR			TEM, PSD	TEM, PSD
150	150	NR	50	BOL Nimbus GDL	PC, EIS	

PC = Polarization curve.

ECSA-HUPD = ECSA using Hydrogen Underpotential Deposition.

SEM = Scanning electron micrograph.

 $TEM = Transmission \ electron \ micrograph.$

PSD = Particle size distribution via TEM.

NC, USA) using 50 cm² cell hardware from Fuel Cell Technologies, Inc. (Albuquerque, NM, USA) with solid plates with 14-channel serpentine flow fields as used by Baker *et al.*³² Cell geometries of 5 cm² (differential cell configuration) and 50 cm² (integral cell configuration) were tested in the 50 cm² hardware with the inactive areas being masked by gasketing. Both cell sizes were sealed using a polyurethane gasket with the 50 cm² cell using a 0.3 μm Kapton° sub-gasket as additional edge protection for the MEA, which reduced the active geometric area of the 50 cm² cell to 47.8 cm². Sealing clamping pressure was achieved by torquing the cell hardware bolts to 60 in-lb.

A sheet of unused MEAs from the original fuel-cell stack production were provided by Nimbus Power Systems (Groton, CT, USA), which served as BOL samples of the stack MEAs. The EOL MEAs and gas-diffusion layers (GDLs) were harvested from the stack cells. For the 50 cm² EOL cells, the GDLs from the corresponding cell was used in the cell testing. The cathode GDL (cGDL) contained a microporous layer (MPL), which left a residue on the MEA when the layers were separated. The anode GDL (aGDL) did not contain an MPL, which resulted in a clean separation of the aGDL and MEA. For 50 cm² BOL cells, OEM GDL materials (Toray® TGP-H-60 for the anode and Sigracet® 25AC for the cathode) were provided by Nimbus Power Systems. These GDLs are ideal for WTP cells and not necessarily solid plates since they are hydrophilic and do not contain any hydrophobic treatments to mitigate GDL flooding. Sigracet 22BB (SGL Carbon SE, Wiesbaden, DE) was used as the GDL material for the 5 cm² cells. The 22BB GDLs are carbon papers that have been PTFE treated and contain an additional MPL to make them hydrophobic, a necessity for solid-plate cells.

BOL MEAs were activated and conditioned using the Million Miles Fuel Cell Truck (M2FCT) protocol based on the work of Kabir *et al.*³³ EOL MEAs were conditioned using the M2FCT protocol prior to operation and electrochemical characterization. Electrochemical characterization for all cells consisted of H₂-N₂ cyclic voltammetry, polarization, EIS, and mass activity using the built-in test stand load box and potentiostat, which were all measured under fully humidified conditions to mimic the wet conditions imposed by the WTPs under operation.³⁴ The polarization and impedance spectra were measured at a cell temperature of 80 °C

at an absolute pressure of $150\,\mathrm{kPa}$ using H_2 -air at 100% relative humidity, with the impedance response being measured galvanostatically from $10\,\mathrm{mHz}$ to $10\,\mathrm{kHz}$ with $10\,\mathrm{points}$ per decade and using a current perturbation amplitude that corresponded to $15\,\mathrm{mV}$ estimated from the total polarization resistance. The reactant gas flow rates for the polarizations using H_2 and air were fixed at $1000\,\mathrm{and}$ 3000 sccm, respectively for the $5\,\mathrm{cm}^2$ differential cells. The flowrates for the $50\,\mathrm{cm}^2$ MEA were based on stoichiometric flow with coefficients of $1.5\,\mathrm{and}$ 2, for the anode and cathode respectively. After electrochemical characterization, MEA samples were further characterized using SEM, and STEM.

The stacks operated at ambient exhaust pressures in the field, but when the polarization curves were measured during maintenance, the recorded exhaust pressures varied. To determine the effect of pressure on the cell performance, the single-cell polarization curves were measured at ambient pressure, which was achieved by disabling the back pressure control, and at a constant gas pressure, which was regulated by setting the back pressure to 150 kPa absolute. Cells were also operated under temperatures ranging from 60 to 80 °C with cathode air flow stoichiometric ratios of 1.25, 1.5, and 2. Parametric studies of cell performance as a function of pressure, temperature, and cathode gas flow are included in the Supplemental Material.

Imaging and particle size procedure.—Scanning transmission electron microscopy (STEM) was performed using a JEOL JEM-ARM200F NEOARM operated at 200 kV on thin slices of membrane electrode assembly cross-sections prepared using diamond-knife ultramicrotomy. The experiments were conducted using a high-angle annular dark field (HAADF) detector. Samples were exposed to a beam shower before experiment acquisition to reduce hydrocarbon contamination.

Particle size measurement was assessed from HAADF-STEM images acquired using specific settings which allowed a larger depth of field. Images in each region of the electrode: bottom (close to the membrane/catalyst layer interface), middle, and top (close to the gas diffusion layer) were acquired to assess discrepancies in the size distributions across the electrode. Following the acquisition, images were analyzed, and particle sizes were measured following the workflow described in Yu et al.³⁵

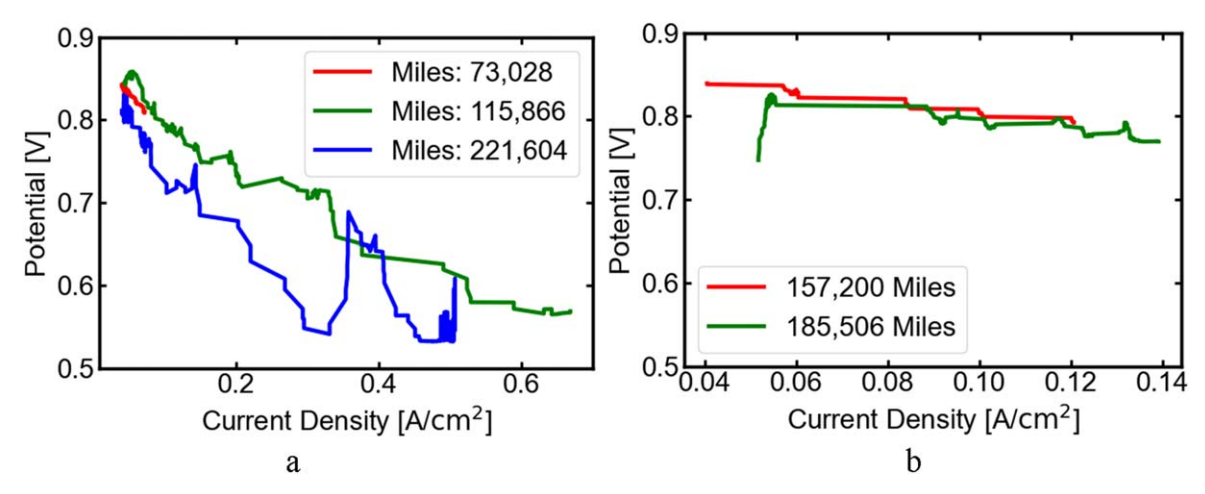


Figure 2. Average polarization curves derived from the provided stack maintenance data at multiple timepoints for both (a) FC4 and (b) FC12.

Results

Stack data analysis.—The performance metrics for the buses were only taken when the bus came in for maintenance, leading to irregular intervals when data was added to the database. For FC4, most of the data was taken near the end of life, with a few timepoints taken earlier. For FC12, unfortunately only two timepoints with polarization data were provided. The comparison between both buses is provided in Fig. 2.

If the anode backpressure is not used as a filter for FC4, we obtain the polarization curves in Fig. S3 in the SI. Figure 3 demonstrates a minimal difference in the performance of the two stacks for FC4, highlighting the symmetry of the system. Due to the similar performance of the two stacks from FC4, the focus of the analysis is on stack A with the expectation that stack B performs similarly.

One interesting characteristic of Fig. 3 is the variation in the power outputs provided between 115 k miles and 221 k miles at 0.3 A cm⁻² and 0.45 A cm⁻². Since the cells within the stack are connected in series, the total current through them is the same and the total power output is given by

$$P = iCVA$$
 [1]

where V is the average voltage difference across one cell, C is the number of cells in both stacks, i is the current density, and A is the active area of the cells. The power output drops from 52 to 40 kW at 0.3 A cm $^{-2}$ after 115 k miles and 221 k miles, respectively, where both are below the power threshold required for bus operation (60 kW). At 0.45 A cm $^{-2}$, though, power goes from 69 to 57 kW, which would have resulted in the bus being decommissioned at 221 k miles with <60 kW power output. Although the peak power output of the stack would be at a slightly higher current density and depends on hybridization, these trends display the overall decline of the performance of the stacks until the eventual decommissioning due to their inability to meet the threshold power requirement.

As the data is provided for every 10 cells, we can additionally compare polarization curve data for cells near the ends of the stack to cells near the center. As seen in Fig. 4, the center of the stack tends to perform worse than the ends at higher current densities, and this gap only widens over the lifetime of the device. From the layout of the stacks, this is possibly due to either heat management issues from coolant water or the reactants inadequately reaching the center of the stacks relative to the ends. Both the cooling water and the reactants move from the ends of the stacks towards the center (see Fig. S1), so the cooling water increases in temperature (reducing effectiveness) and the reactant flow-rate decreases (flow maldistribution). This mechanism can be mitigated using shorter stacks that allow for improved heat exchange with the cooling system and more uniform reactant flow. Other mitigation strategies include different

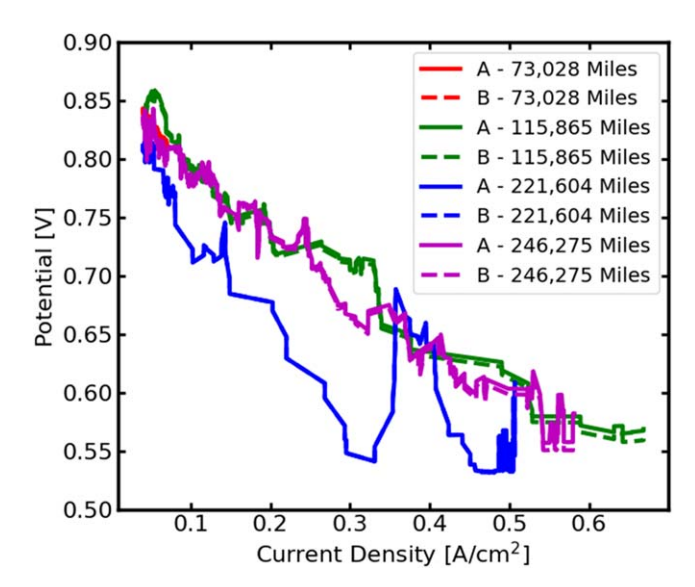


Figure 3. The polarization curves taken for four different time points over the lifetime of FC4. The performance is very similar for both stacks (solid and dotted lines), coinciding indistinguishably in all except the 115 k miles case at higher current densities.

inlet flow arrangements, increasing the number of inlet/outlet stack ports for the reactant streams, and changing the manifold types.

Single-cell testing.—Cell polarization curves were measured using a cell constructed from BOL materials and MEAs and GDLs extracted from the stack. Electrochemical characterization was performed on stack cells 7, 74, 150, 165, 270, 271, and 281. The polarization curves from the 5 cm² and 50 cm² cells are shown in Figs. 5a and 5b respectively. As expected, the 5 cm² cells with 22BB GDLs exhibit higher performance (especially at higher current densities), since these GDLs have hydrophobic treatments, which are preferable for these solid-plate cells. EOL cells from the stack exhibited lower performance when compared to polarization curves from BOL cells. Figure 5a compares the performance of two 5 cm² areas in difference locations of the same MEA: 271-1 is at the anode inlet and 271-4 is at the cathode outlet. The minimal difference in the polarization curves of the two locations, 271-1 and 271-4, illustrates that the performance loss within each cell is extremely uniform with the EOT cells from different locations exhibiting identical performance. To further assess the spatial distribution of cell performance within a 420 cm² cell, 50 cm² MEAs and GDLs were taken from region 1/6 (cathode inlet) and region 3/4 (cathode outlet) of cell 165

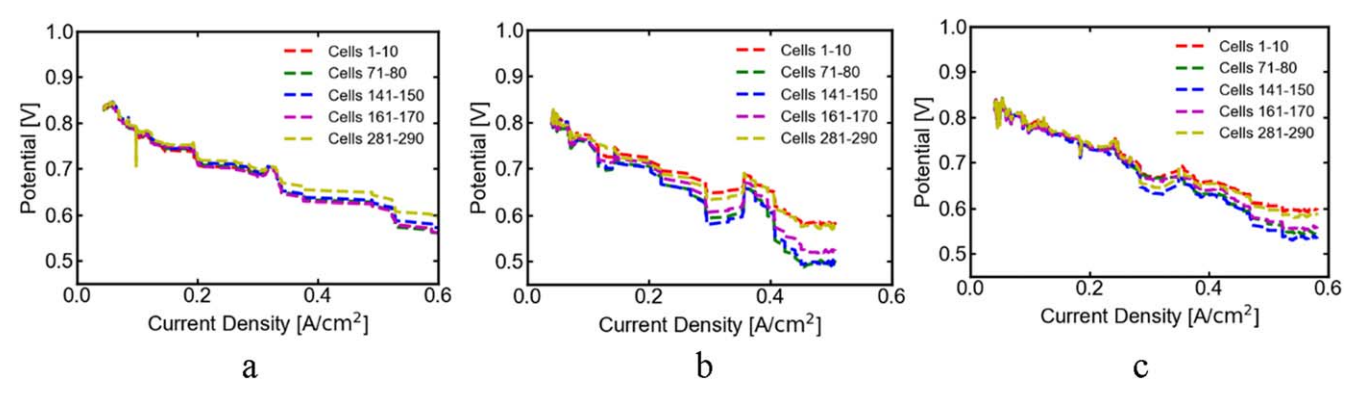


Figure 4. The polarization curve data for (a) 115 k miles, (b) 221 k miles, and (c) 246 k miles for FC4. The middle cells (such as Cells 141–150) tend to perform worse compared to either end of the stack (such as Cells 1–10 and Cells 281–290).

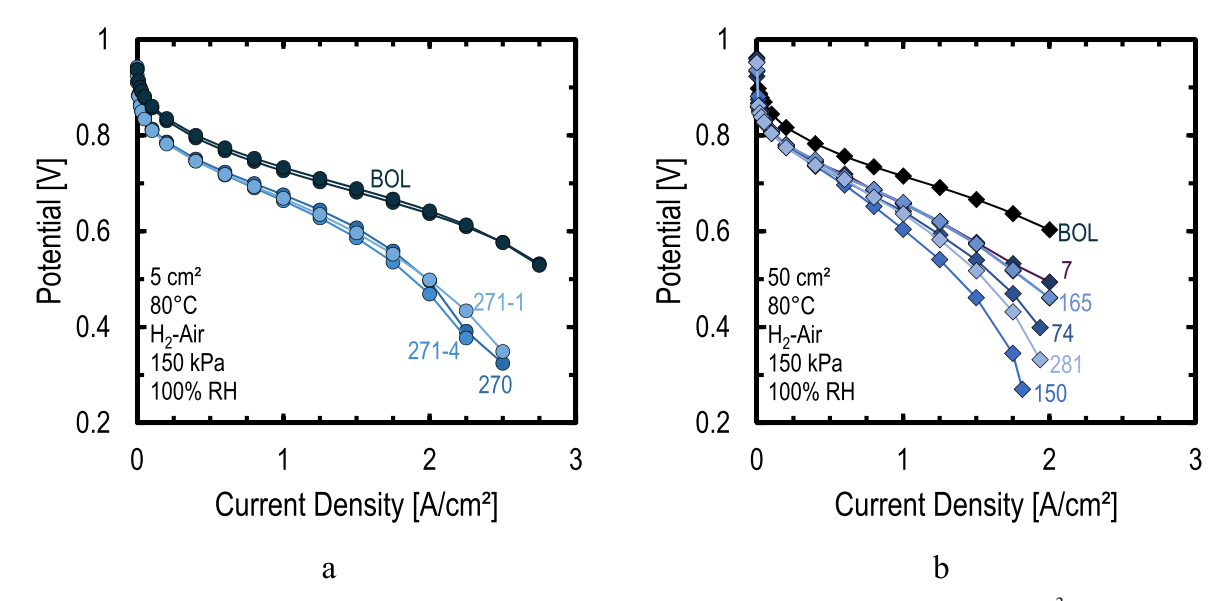


Figure 5. Experimentally observed polarization curves of BOL MEAs and MEAs extracted from the PEMFC stack in (a) 5 cm² cells using Sigarcet^{*} 22BB GDLs for both the anode and the cathode and (b) 50 cm² MEAs using GDLs removed from the corresponding cell with fresh GDLs used for the BOL cell.

to evaluate localized performance losses. Impedance spectra measured at low and high current densities suggested local variations within a cell did not yield significant changes in overall performance (see Fig. S4). This consistently implies that the local operating conditions across the active area, and from cell-to-cell, were relatively uniform, which is due in part to the unique watermanagement enabled by the WTPs which prevent local fuel starvation and provide uniform humidification.

Figure 5b compares the EOL of various cells from FC4 stack A, where the mass-transport-limited regime exhibits higher losses for some MEAs than others. Moreover, there was no clear trend of middle cells (150 and 165) being worse than end cells (7 and 281). Figure S5 shows the EOL performance difference more explicitly with significant mass transport loss variation between the cells. This variation can be attributed to the use of solid plates instead of WTP in this testing and also due to MPL residue remaining on the cathode after extraction of the EOL MEAs.

ECSA was measured from the BOL and EOL stack cells, which showed a significant loss from an initial BOL ECSA of $75.3 \pm 7.0 \,\mathrm{m^2 g^{-1}}$ to an EOL value of $23.7 \pm 2.1 \,\mathrm{m^2 g^{-1}}$. The EOL ECSA was consistent throughout all EOL stack MEAs. The EIS response was measured at every steady-state current density in the polarization curve. Select spectra are shown for current densities of $400 \,\mathrm{mA \ cm^{-2}}$ and $1 \,\mathrm{A \ cm^{-2}}$ in Fig. 6. In Fig. 6a, BOL was observed to yield the lowest impedance with a majority of EOL cells having similar performance with the exception of cell 150, which

showed significant increases in cell impedance at both high and low frequencies. The disparity in impedance was greater at high current densities, as shown in Fig. 6b, where the observed impedance in cell 150 was significantly larger than all other cells tested. These EIS results agree with the results shown in the SI and show the cell to cell performance variability in the mass transport region.

SEM characterization.—SEM images of MEAs were taken from BOL and EOL cells 7, 150, 165, 271, and 281. In Fig. 7, the formation of a platinum band was observed in EOL samples. Images from BOL and the best and worst performing EOL cells, which were cells 7 and 150 are illustrated in Figs. 7a–7c respectively. EOL layer thickness of the aCL, Membrane (M), and cCL shown in Figs. 7d–7f respectively, suggest that loss of cCL occurred to the greatest extent followed by the aCL with the membrane remaining about the same thickness as BOL. The performance from cell 7 was the best observed from the stack while cell 150 was the worst. Layer thicknesses did not correlate to observed cell performance indicating that the transport losses observed in these cells due to any degradation are smaller than the cell to cell variability observed between the various MEAs extracted from the stack and tested in solid plates.

To determine the role of Pt dissolution/aggregation in the differences in performance between middle and end cells, we took Pt particle size measurements for both cell 7 and cell 150 using HAADF-STEM as illustrated in Fig. 8. Although some larger Pt

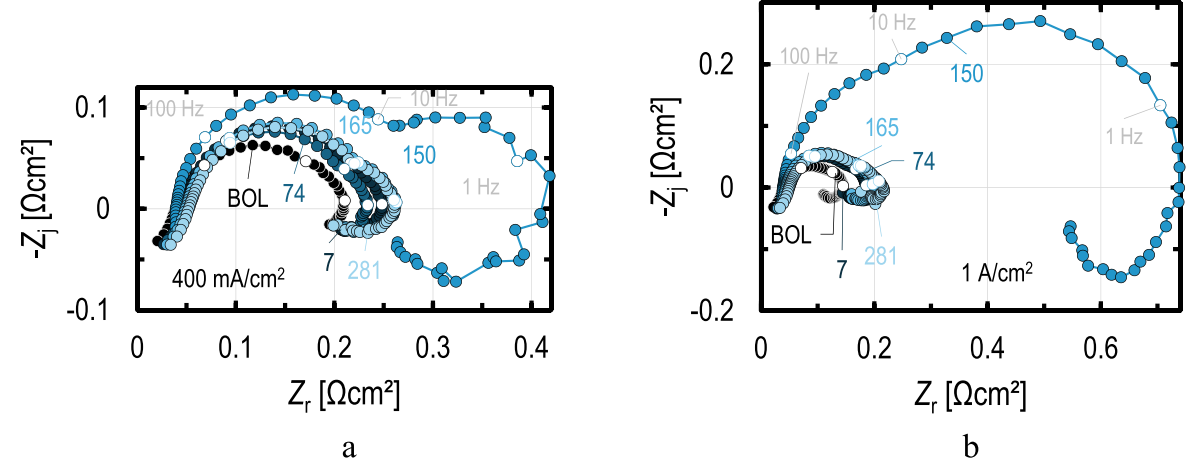


Figure 6. EIS spectra obtained from 50 cm² cells at (a) 400 mA cm⁻² and (b) 1 A cm⁻² Performance was best using BOL materials. Cells from 7, 165, and 281 are slightly worse than BOL, but relatively consistent while cell 150 showed significantly enhanced degradation in the mass transport region.

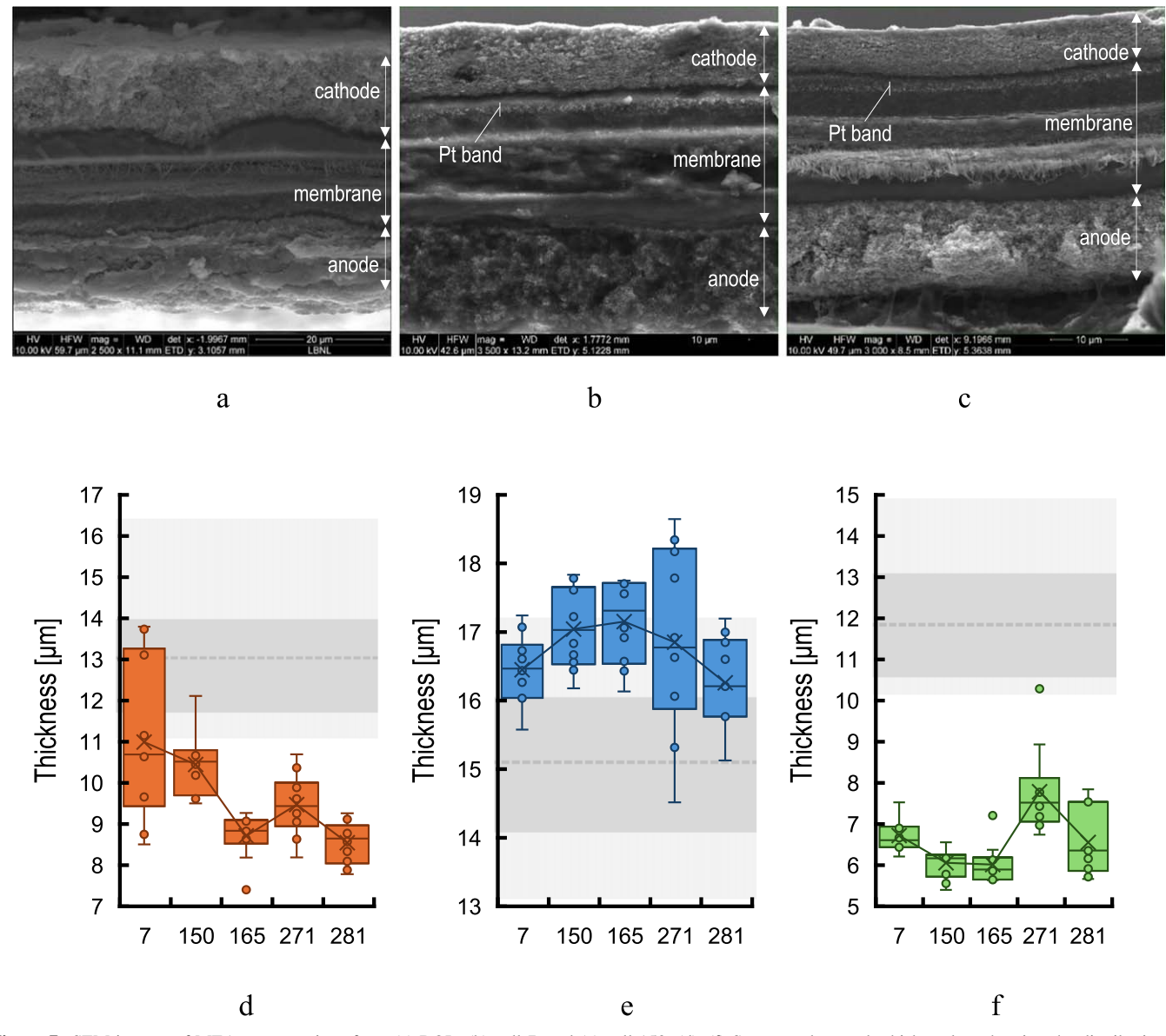


Figure 7. SEM images of MEA cross sections from (a) BOL, (b) cell 7, and (c) cell 150. (d)–(f) Summary box-and-whisker plots showing the distribution of thicknesses obtained from SEM images for (d) aCL, (e) M, and (f) cCL. The BOL measurements are the shaded regions for the box values and dotted horizontal lines for the whisker values.

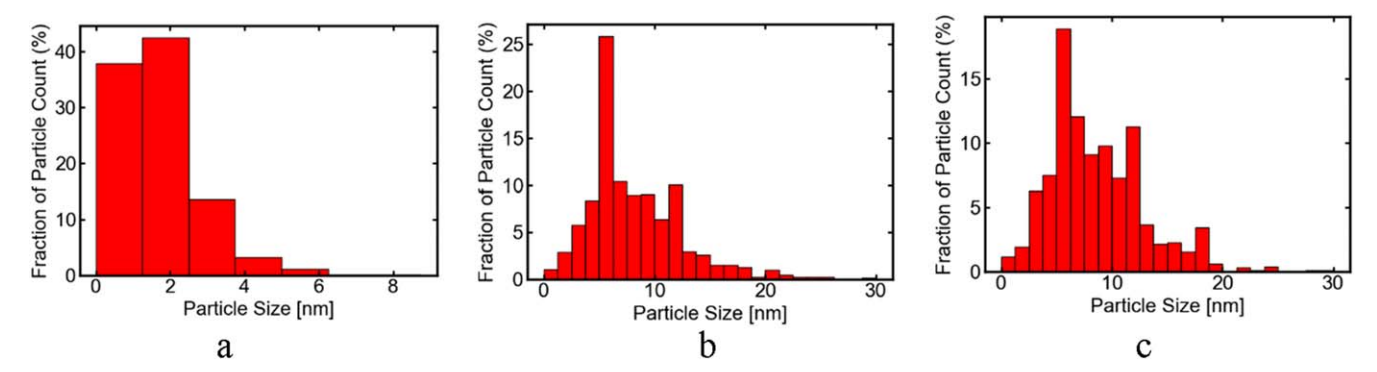


Figure 8. Particle-size distributions for (a) BOL with an average particle size of 2.2 ± 1.3 nm, (b) (EOL) cell 7 with an average particle size of 7.6 ± 3.6 nm, and (c) (EOL) cell 150 with an average particle size of 8.2 ± 4.1 nm.

particles can be observed in cell 150 as compared to cell 7, the differences between these cells were within error and significantly greater than BOL.

Another possible degradation mechanism comes from the formation of a Pt band within the membrane, which can influence membrane degradation and cause ECSA loss. ^{36,37} However, STEM images of Pt bands in the membranes of cells 7 and 150 show little differences in the thicknesses of the Pt band (as depicted in Fig. 9).

Discussion

After 25,000 h and 221 k miles of operation, although the power output of the bus system decreased to the point of decommissioning the fuel-cell bus, the degradation of the MEAs does not explain this dramatic loss in stack power. The performance measured in the stacks in the buses is dramatically different than what is measured in lab cells using the same MEAs. For example, with FC4, the polarization curve at 0.3 A cm $^{-2}$ for the data at 221 k miles yields an operating voltage of 0.55 to 0.6 V, while the polarization curve taken with EOL MEA materials yields an operating voltage of 0.75 V, a power increase of at least 20%. This result occurs despite the EOL data being taken after further degradation of the fuel cells from 221 k miles.

There is no evidence of substantial membrane thinning (Fig. 7) and the OCV is relatively constant (Fig. S6) and the hydrogen crossover rates are also low (Fig. S7a). The lack of membrane degradation is not surprising in WTP cells since this passive water-management technology results in the entire active area being maintained at close to 100% RH, with minimal RH cycling. Therefore, two major accelerating conditions for membrane degradation, low RH and RH cycling, are effectively mitigated in WTP

cells.¹⁷ A direct comparison of membrane degradation in WTP cells and conventional solid-plate cells has been demonstrated previously.³⁸

However, there is some evidence of thinning of the catalyst layers, especially the cathode catalyst layers. This is expected, since the cathode potential is greater than the thermodynamic potential for carbon corrosion. Additionally, the high-RH environment of WTP cells should promote carbon corrosion. However, there is no strong evidence of severe cathode thinning, as one might expect from the reverse current mechanism that results during uncontrolled start/stop cycles. This is because UTC Power implemented multiple start/ stop-decay-mitigation strategies, which have been summarized elsewhere. Is since UTC Power was the first to discover start/stop decay, they were also the first to implement these mitigation strategies, which are now commonly used in most fuel-cell vehicle applications. Because WTP cells suck liquid water into the porous plates, local flooding is prevented and local carbon corrosion due to local fuel starvation is also mitigated.

From CV and SEM measurements, the CLs exhibited loss of ECSA and layer thicknesses. The ECSA shows a monotonically increasing dependance on the cCL thickness, which is shown in Fig. S7b in the SI. The loss of ECSA appears to be primarily due to the growth of the Pt particles due to Ostwald ripening (accelerated by higher temperature), platinum dissolution due to potential cycles, and loss of carbon support due to the aforementioned corrosion. As these mechanisms are further accelerated at the increased RH encountered with the use of WTPs, this reduction in Pt surface area is expected. Although these buses were hybrids, the fuel cells underwent extensive power/voltage cycles since the batteries were not large. However, UTC Power did practice voltage clipping to

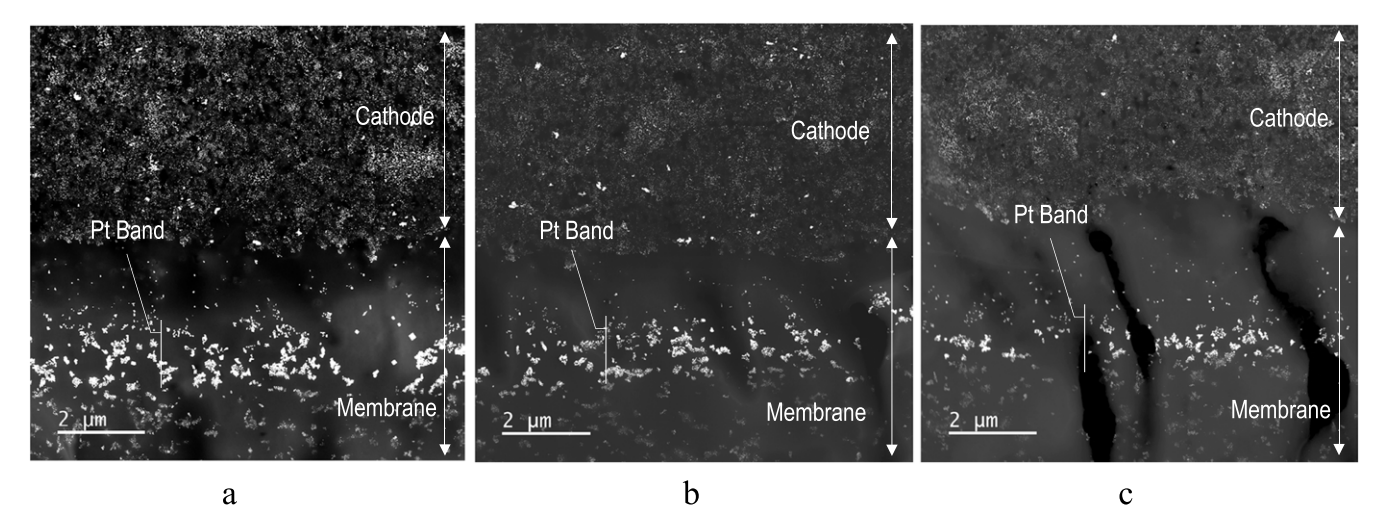


Figure 9. The Pt bands (light particles) taken from STEM sampled from (a) cell 7, region 1 with an average thickness of 1.5 μ m, (b) cell 7, region 6 with an average thickness of 1.4 μ m, and (c) cell 150 with an average thickness of 1.2 μ m.

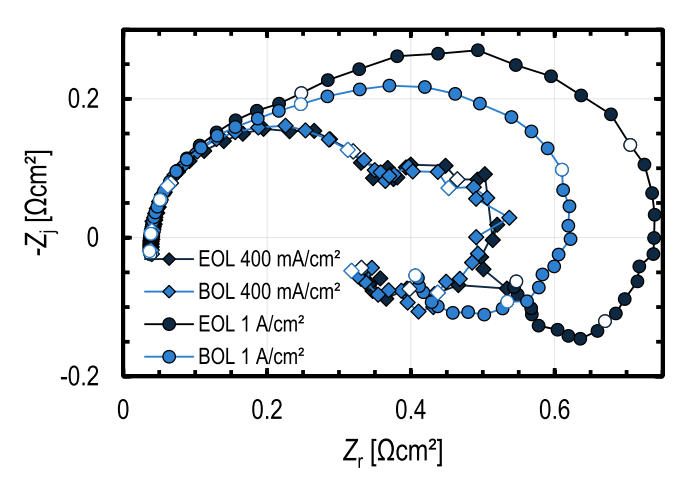


Figure 10. Impedance spectra obtained at 400 mA $\rm cm^{-2}$ and 1 A $\rm cm^{-2}$ using EOL and BOL GDLs. MEAs were taken from cell 150.

avoid open-circuit conditions, which does mitigate Pt growth due to potential cycles. Additionally, the performance loss related to ECSA loss corresponds to only about 50 mV at 0.5 A cm $^{-2}$ consistent with $\approx\!65\%$ ECSA loss (Fig. S8). All the tested EOL MEAs gave a voltage $>\!0.7$ V at 0.5 A cm $^{-2}$ (see Fig. 5) when tested in $50~\text{cm}^2$ cells, whereas these cells had a voltage $<\!0.6$ V at 0.5 A cm $^{-2}$ when operated in the bus. Therefore, it is reasonable to conclude that the larger particle sizes while responsible for $\approx\!50~\text{mV}$ loss at 0.5 A cm $^{-2}$, cannot be the cause of the $>\!150~\text{mV}$ loss observed in the buses.

Since changes in the catalyst layer and membrane cannot explain the voltage losses observed in the buses, attention was paid to differences in the gas diffusion layer and other system variables. While the buses were large systems operated using WTPs, the BOL and EOL MEAs were tested in single cells using solid plates and either fresh hydrophobic (5 cm² cell) or EOL (50 cm² cell) GDLs. This leads to the conclusion that balance of plant and system issues, or GDL degradation could be the root cause of the loss of power observed in the bus systems.

The influence of GDL degradation was quantified by performing cell studies with an EOL MEA with EOL and BOL GDL materials, showing only little differences (see Fig. S9). Cell 150 was observed to have the lowest performance, which could not be explained by ECSA or SEM images and was therefore used for this study. The impedance spectra were compared between the cell using BOL and EOL GDL materials, which is shown in Fig. 10.

At lower current densities, the spectra showed good superposition between EOL and BOL GDL materials. At higher current densities, the spectra exhibited increased mass-transport effects indicated by the larger lower-frequency loops. Analysis suggests that a mild negative effect on MEA performance was observed due to the GDL, which was insufficient to explain the origin of the lower performance of cell 150. Therefore, the mass transport variations observed between the different cells are more likely due to cell to cell variability arising from cell extraction (MPL residue on cathode catalyst layer) and not due to any systematic GDL degradation. It should also be noted that low-frequency inductive features in the measured impedance spectra were observed in both Figs. 6 and 10, which used 50 cm² integral flow fields. These features have been attributed to various mechanisms including water transport, 43-45 PtO formation in the cCL,46 and hydrogen-peroxide reaction intermediates.4

In checking for failure mechanisms through other avenues, although the data does not extend to open circuit, we tried to capture the near open-circuit behavior. As open-circuit voltage performance does not typically depend on anode backpressure, all of the polarization curve data is utilized instead of only a filtered subset. The data was truncated between 0.05 and 0.4 A cm⁻² and voltage between 0.6 V to 0.9 V and the voltage extrapolated to zero current using straight lines to examine for a trend (lack of data in the kinetic region did not enable Tafel fitting). As shown in Fig. S6 in the SI, although the found open-circuit voltages are quite noisy, the overall lifetime open-circuit voltage was relatively stable at 0.83 ± 0.02 V (low due to linear extrapolation instead of using a Tafel slope). The open circuit voltage trend was observed in addition to the absence of significant membrane thinning at EOL, as depicted in Fig. 7 as well as low hydrogen crossover rates demonstrated in Fig. S7a, all of which demonstrate little membrane thinning. This demonstrates how a membrane can be maintained at nearly ideal performance by keeping it hydrated, even with a lack of radical scavengers, such as Cerium. 48 This data bodes very well for the overall performance of fuel cells with radical scavengers especially if drier conditions and RH gradients can be mitigated.⁴

EOL power output.—The given polarization data was used to estimate the power output of the cell at every current density by fitting a quadratic function to each curve in order to force a maximum, as demonstrated in Fig. 11a. The power expression in Eq. 1 can be modified to demonstrate a quadratic dependence where a linear polarization curve is involved. Here, it should be noted that the quadratic fit for 73 k miles was performed with a current density range of less than 0.1 A cm⁻², so the resulting fit should not be

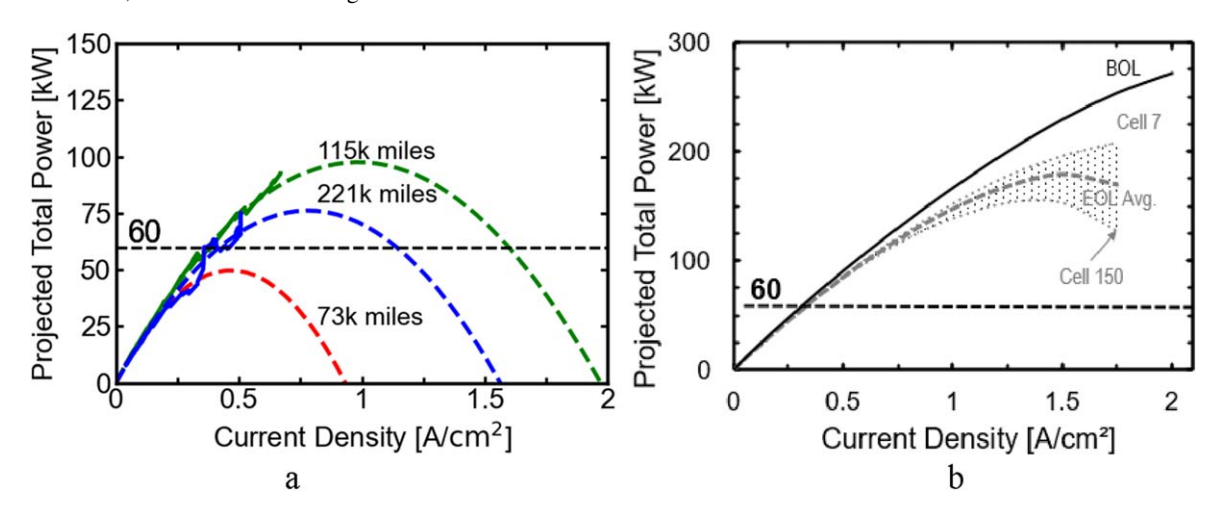


Figure 11. Power curves observed from (a) data given during the lifetime of the bus and expanded using a quadratic fit and (b) projected total power output of a two-stack power plant operated at ambient pressure. The projected total power curves using the polarization data from the best and worst cell were also calculated to suggest maximum and minimum EOL total power output. The EOL average was obtained by averaging all the 50 cm² polarization curves. The minimum required power plant power output is indicated by the horizontal 60 kW line.

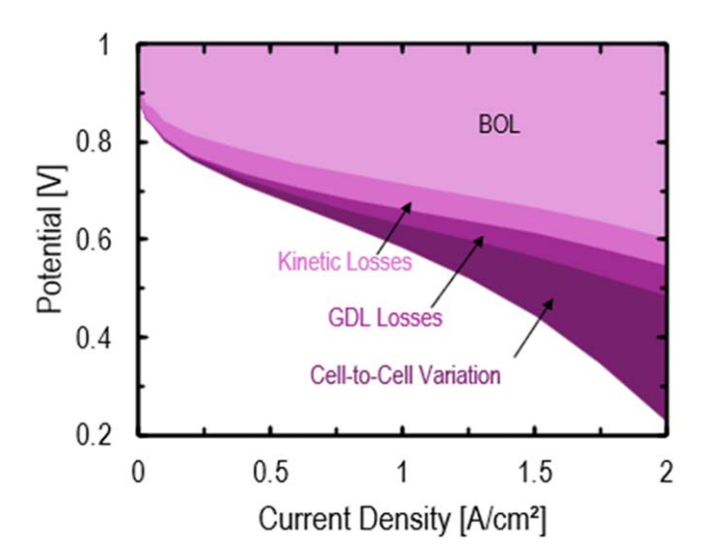


Figure 12. Contributions to the total cell losses were estimated by comparing polarization curves obtained from cells recovered from the stack cell assembled with new materials. Kinetic losses were estimated from the difference in polarization between the BOL and EOL performance estimated from OCV to 100 mA cm⁻². GDL losses were estimated from the polarization data from assembling EOL stack MEAs with EOL and BOL GDL materials. Stack distribution losses were estimated from polarization differences between the best and worst EOL stack cells, which were cell 7 and cell 150, respectively.

trusted, but has been included for completeness. The polarization curves were used to estimate the power output of the two-stack power plant (120 kW rated power) contained within a bus. The power curves obtained from the EOL 50 cm² MEAs were corrected for back pressure and extrapolated using the total estimated active area of the two stacks, and are shown in Fig. 11b. Estimates of the total power output suggests a 6 to 10% power loss, which is well below the system-observed decommissioning power loss of 50%. The polarization curves shown in Fig. S10, where an EOL cell was operated at ambient and at 150 kPa back pressure, were used to perform a pressure correction and to estimate the EOL stack potential. Ambient pressure operation yielded a reduction in cell potential of 25 mV at open circuit up to 50 mV at operating current densities. Figure S11 illustrates the power curves for all the tested 50 cm² cells shown in Fig. 5b.

The EOL projected power output accounts for performance losses in the 50 cm² cell tested. Although the maximum power of the parabolas in Fig. 11a tends towards 60 kW (any lower would indicate bus failure), the power curves projected from Fig. 11b instead suggest ample power available in the fuel cells to meet performance requirements.

Utilizing the total potential losses between cells 7 and 150 (see Fig. S5), we can break down the differences between BOL and EOL cells through expected mechanisms as in Fig. 12. Kinetic losses were estimated from the difference in polarization for relatively low current densities. GDL losses were evaluated from the differences in the polarization curves between BOL and cell 7 at EOL after accounting for the kinetic loss. Cell-to-cell variation losses were estimated from the differences in the polarization between the best and worst cells in the stack at EOL. These results are consistent with the observed catalyst and GDL degradation as discussed above but not consistent with the power loss observed in the bus stack. Moreover, these losses were insensitive to the various cell operating parameters including temperature and cathode flow rate (see Fig. S12).

Conclusions

The results of this study provide valuable insights into PEMFC degradation during extended operation in fuel-cell buses. The polarization curves and electrochemical impedance spectroscopy

(EIS) data demonstrate a clear decline in performance from BOL to EOL cells. The observed degradation can be explained by well-known decay mechanisms. This loss of performance can be primarily attributed to a loss of ECSA, due to growth of the Pt particles, as well as some loss of Pt to a band in the membrane. There were minimal changes to the membrane, and catalyst-layer thinning was uniform throughout the active area and cell location, possibly aided by high catalyst loading. These two results may be attributed to the use of water-transport plates (WTPs), which passively maintain uniform (≈100% relative humidity) conditions with minimal liquid water flooding.

Despite this cell degradation, the EOL fuel-cell components tested individually continued to perform at a level sufficient for meeting the power demand specifications of the buses of the Alameda Contra Costa Transit District. The greatest differences, instead, were between the data taken during the lifetime of the bus and the EOL polarization curves, which utilized fresh GDLs. This signifies the majority of the performance losses were due to sources outside of the membrane and catalyst layer. One possibility is a change in the system balance of plant, meaning supporting hardware not inclusive of the fuel cell stacks, such as degradation in the air blower or seals, which could result in the poor performance observed in the buses. More work is required to determine the actual root cause of this significant discrepancy. Future exploration could include testing of entire systems and/or stacks across the entire voltage range, which are beyond current capabilities.

Outside of the possible limitations of the stacks, the analysis completed demonstrates that both the membrane and the catalyst layers retain their BOL performance to a large degree and could continue to be utilized. After reaching EOL (above 25,000 h), the degradation of the MEA accounted for only a 50 mV decrease at 1 A cm⁻². Additional optimization methods such as utilizing radical scavengers and pressurizing inlet flows would enhance the performance of the MEA even further. With these design principles in mind, the findings and data analysis of this study provide a basis for future improvements in material design and operational strategies to extend the lifetime of PEMFCs in real-world applications.

Acknowledgments

The authors would like to thank Jose Vega, James Souza, and Cecil O. Blandon from the Alameda Contra Costa Transit District for their help in providing the data taken over the lifetime of the fuel cell buses. This work was supported by the Hydrogen and Fuel Cell Technologies Office (HFTO), Office of Energy Efficiency and Renewable Energy, U.S. Department of Energy (DOE) through the Million Mile Fuel Cell Truck (M2FCT) consortia, technology managers G. Kleen and D. Papageorgopoulos, under Contract Number DE-AC02-05CH11231. Electron microscopy research was supported by the Center for Nanophase Materials Sciences (CNMS), which is a U.S. Department of Energy, Office of Science User Facility at Oak Ridge National Laboratory. All opinions expressed in this article are of the authors' and do not necessarily reflect the policies and views of the DOE.

ORCID

Harsh Srivastav https://orcid.org/0000-0002-5566-3720 Arthur Dizon https://orcid.org/0000-0002-7872-1399 Mike L. Perry https://orcid.org/0000-0003-3313-8498 Catherine M. Weiss https://orcid.org/0000-0001-6688-3246 Douglas I. Kushner https://orcid.org/0000-0002-3020-7737 Dave A. Cullen https://orcid.org/0000-0002-2593-7866 Adam Z. Weber https://orcid.org/0000-0002-7749-1624 Rangachary Mukundan https://orcid.org/0000-0002-5679-3930

References

- 1. Energy.govFuel Cells, (2025-03-17), https://energy.gov/eere/fuelcells/fuel-cells.
- R. Borup et al., "Scientific aspects of polymer electrolyte fuel cell durability and degradation." *Chem. Rev.*, **107**, 3904 (2007).

- L. Fan, Z. Tu, and S. H. Chan, "Recent development of hydrogen and fuel cell technologies: a review." *Energy Reports*, 7, 8421 (2021).
- N. Sazali, W. N. Wan Salleh, A. S. Jamaludin, and M. N. Mhd Razali, "New perspectives on fuel cell technology: a brief review." *Membranes (Basel)*, 10, 99 (2020).
- Global Hydrogen Review 2022—Analysis (IEA), (2025-03-18), https://iea.org/reports/global-hydrogen-review-2022.
- Energy.govHydrogen Production: Electrolysis, (2024-12-09), https://energy.gov/eere/fuelcells/hydrogen-production-electrolysis.
- Electrolysis for Green Hydrogen Production, Linde, (2024-12-09), https://linde.com/clean-energy/our-h2-technology/electrolysis-for-green-hydrogen-production.
- S. Shiva Kumar and H. Lim, "An overview of water electrolysis technologies for green hydrogen production." *Energy Reports*, 8, 13793 (2022).
- N. A. A. Qasem and G. A. Q. Abdulrahman, "A Recent Comprehensive Review of Fuel Cells: History, Types, and Applications." *International Journal of Energy Research*, 2024, 7271748 (2024), 10.1155/2024/7271748.
- Toyota Fuel Cell Electric Vehicles/Toyota Europe (Toyota EU), (2024), https://toyota-europe.com/electrification/fcev.
- 2023 Nexo Fuel Cell|Vehicle Overview|Hyundai USA, (2024-12-09), https:// hyundaiusa.com/us/en/vehicles/nexo.
- 2025 Honda CR-V e:FCEVIHydrogen Fuel Cell Vehicle, (2024-12-09), https://automobiles.honda.com/cr-v-fcev.
- AC Transit Fuel Cell Bus Longevity Study Report Summary/FTA, (2025-03-30), https://transit.dot.gov/research-innovation/ac-transit-fuel-cell-bus-longevity-study-report-summary.
- Zero Emission Bus Technology AnalysislAlameda-Contra Costa Transit District, (2025-03-30), https://actransit.org/zebta.
- AC Transit Bus RosterlAlameda-Contra Costa Transit District, (2025-03-30), https://actransit.org/index.php/ac-transit-bus-roster.
- GORE-SELECT® Membranes(PEM) for Fuel Cells/Gore, (2024-12-09), https://gore.com/products/gore-select-membrane.
- A. Z. Weber and R. M. Darling, "Understanding porous water-transport plates in polymer-electrolyte fuel cells." J. Power Sources, 168, 191 (2007).
- X. Wang, X. Huang, L. J. Bonville, H. R. Kunz, M. L. Perry, and D. Condit, "Impact of in-cell water management on the endurance of polymer electrolyte membrane fuel cells." J. Electrochem. Soc., 161, F761 (2014).
- B. Sreenivasulu, G. Vasu, V. D. Rao, and S. V. Naidu, *International Journal of Applied Science and Engineering*, 11, 1 (2013).
- K. Jiao, B. Wang, Q. Du, Y. Wang, G. Zhang, Z. Yang, H. Deng, and X. Xie, "Chapter 3 - Experimental characterization and diagnostics." Water and Thermal Management of Proton Exchange Membrane Fuel Cells (Elsevier, Amsterdam) 67 (2021).
- D. Hao, J. Shen, Y. Hou, Y. Zhou, and H. Wang, "An improved empirical fuel cell polarization curve model based on review analysis." *International Journal of Chemical Engineering*, 2016, 4109204 (2016).
- C. Zhang, W. Li, M. Hu, X. Cheng, K. He, and L. Mao, "A comparative study of using polarization curve models in proton exchange membrane fuel cell degradation analysis." *Energies*, 13, 3759 (2020).
- B. Padha, S. Verma, P. Mahajan, and S. Arya, "Electrochemical impedance spectroscopy (EIS) performance analysis and challenges in fuel cell applications." *J. Electrochem. Sci. Technol.*, 13, 167 (2022).
- Z. He and F. Mansfeld, "Exploring the use of electrochemical impedance spectroscopy (EIS) in microbial fuel cell studies." *Energy Environ. Sci.*, 2, 215 (2009).
- F. Haimerl, S. Kumar, M. Heere, and A. S. Bandarenka, "Electrochemical impedance spectroscopy of PEM fuel cells at low hydrogen partial pressures: efficient cell tests for mass production." *Ind. Chem. Mater.*, 2, 132 (2024).
- S. M. Rezaei Niya and M. Hoorfar, "Study of proton exchange membrane fuel cells using electrochemical impedance spectroscopy technique—a review." J. Power Sources, 240, 281 (2013).
- B. Najafi, P. Bonomi, A. Casalegno, F. Rinaldi, and A. Baricci, "Rapid fault diagnosis of PEM fuel cells through optimal electrochemical impedance spectroscopy tests." *Energies*, 13, 3643 (2020).
- L. Žnidarič, G. Nusev, B. Morel, J. Mougin, D. Juričić, and P. Boškoski, "Evaluating uncertainties in electrochemical impedance spectra of solid oxide fuel cells." Appl. Energy, 298, 117101 (2021).

- S. Latorrata, R. Pelosato, P. Gallo Stampino, C. Cristiani, and G. Dotelli, "Use of electrochemical impedance spectroscopy for the evaluation of performance of PEM fuel cells based on carbon cloth gas diffusion electrodes." *Journal of Spectroscopy*, 2018, 3254375 (2018)
- H. Yu, M. J. Zachman, C. Li, L. Hu, N. N. Kariuki, R. Mukundan, J. Xie, K. C. Neyerlin, D. J. Myers, and D. A. Cullen, "Recreating fuel cell catalyst degradation in aqueous environments for identical-location scanning transmission electron microscopy studies." ACS Appl. Mater. Interfaces, 14, 20418 (2022).
- A. Kobayashi, T. Fujii, C. Harada, E. Yasumoto, K. Takeda, K. Kakinuma, and M. Uchida, "Effect of Pt and ionomer distribution on polymer electrolyte fuel cell performance and durability," ACS Appl. Energy Mater., 4, 2307 (2021).
- performance and durability." ACS Appl. Energy Mater., 4, 2307 (2021).
 D. R. Baker, D. A. Caulk, K. C. Neyerlin, and M. W. Murphy, "Measurement of oxygen transport resistance in PEM fuel cells by limiting current methods."
 J. Electrochem. Soc., 156, B991 (2009).
- 33. S. Kabir, D. J. Myers, N. Kariuki, J. Park, G. Wang, A. Baker, N. Macauley, R. Mukundan, K. L. More, and K. C. Neyerlin, "Elucidating the dynamic nature of fuel cell electrodes as a function of conditioning: an ex situ material characterization and in situ electrochemical diagnostic study." ACS Appl. Mater. Interfaces, 11, 45016 (2019).
- AST ProtocolsIM2FCT, (2024-12-09), https://millionmilefuelcelltruck.org/ast-protocols.
- H. Yu, M. J. Zachman, K. S. Reeves, J. H. Park, N. N. Kariuki, L. Hu, R. Mukundan, K. C. Neyerlin, D. J. Myers, and D. A. Cullen, "Tracking nanoparticle degradation across fuel cell electrodes by automated analytical electron microscopy." ACS Nano, 16, 12083 (2022).
- N. Ramaswamy, S. Kumaraguru, K. Jarvis, and P. Ferreira, "Improving durability of fuel cells with platinum-rich alloy cathode catalysts." J. Electrochem. Soc., 170, 054504 (2023).
- J. P. Braaten, S. Ogawa, V. Yarlagadda, A. Kongkanand, and S. Litster, "Studying Pt-based fuel cell electrode degradation with nanoscale X-ray computed tomography." J. Power Sources, 478, 229049 (2020).
- X. Huang, X. Wang, J. Preston, L. Bonville, H. R. Kunz, M. Perry, and D. Condit, "Effect of water management schemes on the membrane durability in PEMFCs." ECS Trans., 16, 1697 (2008).
- T. Ous and C. Arcoumanis, "Degradation aspects of water formation and transport in proton exchange membrane fuel cell: a review." *J. Power Sources*, 240, 558 (2013).
- C. A. Reiser, L. Bregoli, T. W. Patterson, J. S. Yi, J. D. Yang, M. L. Perry, and T. D. Jarvi, "A reverse-current decay mechanism for fuel cells." *Electrochem. Solid-State Lett.*, 8, A273 (2005).
- M. L. Perry, T. Patterson, and C. Reiser, "Systems strategies to mitigate carbon corrosion in fuel cells." ECS Trans., 3, 783 (2006).
- R. M. Darling and J. P. Meyers, "Kinetic model of platinum dissolution in PEMFCs." J. Electrochem. Soc., 150, A1523 (2003).
- I. A. Schneider, S. A. Freunberger, D. Kramer, A. Wokaun, and G. G. Scherer, "Oscillations in gas channels: I. The forgotten player in impedance spectroscopy in PEFCs." J. Electrochem. Soc., 154, B383 (2007).
- I. A. Schneider, D. Kramer, A. Wokaun, and G. G. Scherer, "Oscillations in gas channels: II. Unraveling the characteristics of the low frequency loop in Air-Fed PEFC impedance spectra." *J. Electrochem. Soc.*, 154, B770 (2007).
- I. A. Schneider, M. H. Bayer, A. Wokaun, and G. G. Scherer, "Impedance response of the proton exchange membrane in polymer electrolyte fuel cells." *J. Electrochem. Soc.*, 155, B783 (2008).
- B. P. Setzler and T. F. Fuller, "A physics-based impedance model of proton exchange membrane fuel cells exhibiting low-frequency inductive loops." *J. Electrochem. Soc.*, 162, F519 (2015).
- S. K. Roy, M. E. Orazem, and B. Tribollet, "Interpretation of low-frequency inductive loops in PEM fuel cells." *J. Electrochem. Soc.*, 154, B1378 (2007).
- F. D. Coms, H. Xu, T. McCallum, and C. Mittelsteadt, "Mechanism of perfluorosulfonic acid membrane chemical degradation under low RH conditions." ECS Trans., 64, 389 (2014).
- L. Wang, S. G. Advani, and A. K. Prasad, "Degradation reduction of polymer electrolyte membranes using CeO₂ as a free-radical scavenger in catalyst layer." *Electrochim. Acta*, 109, 775 (2013).